Fuel-Rich Premixed *n*-Heptane/Toluene Flame: a Molecular Beam Mass Spectrometry and Chemical Kinetic Study

D.A. Knyazkov[1,2*], N.A. Slavinskaya[3], A.M. Dmitriev[1,2], A.G. Shmakov[1,2], O.P. Korobeinichev[1], and U. Riedel[3]

[1]Voevodsky Institute of Chemical Kinetics and Combustion, Novosibirsk, Russia
[2] Novosibirsk State University, Novosibirsk, Russia
[3]German Aerospace Centre (DLR), Institute of Combustion Technology, Stuttgart, Germany

Abstract

The mole fraction profiles of major flame species and intermediates including PAH precursors are measured in an atmospheric premixed burner-stabilized fuel-rich (φ = 1.75) *n*-heptane/toluene/O_2/Ar flame (*n*-heptane/toluene ratio is 7:3 by liquid volume). These data are simulated with a detailed, extensively validated chemical kinetic reaction mechanism for combustion of *n*-heptane/toluene mixture, involving the reactions of PAH formation. The mechanism is extended with cross reactions for *n*-heptane and toluene derivatives. A satisfactory agreement between the new experimental data on the structure of *n*-heptane/toluene flame and the numerical simulations is observed. The mechanism reported can be successfully used in the models of practical fuel surrogates for reproducing the formation of soot precursors. The analysis of the reaction pathways shows that in the flame of the *n*-heptane/toluene blend (7:3 liquid volume ratio) the reactions dominant for the formation of the first aromatic ring (benzene and phenyl) are as those typical for pure toluene flames. The discrepancies between the measured and calculated species mole fractions are detected as well. The steps for the mechanism improvements are determined on the basis of the sensitivity analysis performed. To our knowledge, the measurements of mole fraction profiles of PAH and intermediates reported here, are the first of its kind and represent an unique data set extremely important for validation of chemical kinetic mechanisms for combustion of practical fuels.

Keywords: formation of soot precursors; chemical kinetic mechanism; *n*-heptane; toluene; molecular-beam mass spectrometry

Introduction

Practical hydrocarbon fuels are complex mixtures of several hundreds of individual species. The kinetics of all of the components and kinetics interactions among them are not fully determined today. In order to establish the optimal composition for a surrogate blends, i.e. simplified reaction models of practical fuels, which mimic the real fuel combustion properties, one needs to specify criteria for choosing appropriate surrogate candidates [1-2] One of these criteria is the Threshold Sooting Index (TSI), an empirical index based on the smoke point. The TSI has been shown to be strongly dependent on the aromatic component fraction of the fuel and is used to compare the tendency of different fuels to soot formation [3]. As TSI is an empirical value, it cannot be used for a validation of chemical kinetic mechanisms developed for simulations of polyaromatic hydrocarbon (PAH) formation in fuels combustion. PAHs are considered to be important soot precursors in combustion processes [4-6]. The profiles of PAH concentrations measured in the flames under different operation conditions can deliver useful information for kinetic mechanism construction.

Different blends and kinetic mechanisms have been recently developed to simulate the combustion of practical fuels [7-9]. These models are mostly established to contain the species from 4 main families of hydrocarbons (*n/i*- paraffins, naphthenes, aromatics) and to predict various combustion characteristics (like ignition delay times, flame speed, mole fraction profiles of flame species, etc.). The

* Corresponding author. E-mail: knyazkov@kinetics.nsc.ru

prediction of pollutant formation, i.e. nitrogen oxides (NO_x), CO_2 and soot, is more complicated problem, due to the much larger size of the required reaction mechanisms (NO_x, PAH) and the complexity of the entire process (PAH). As the mixture of simplest substituted aromatic (C_7H_8, toluene) and "smallest" large *n*-paraffin (*n*-C_7H_{16}, *n*-heptane) used in fuel blends, this combination can be effectively used for an investigation of specifics of PAH formation and growth in engines.

Toluene and *n*-heptane are commonly used as the representatives of aromatics and paraffins in surrogates of gasoline and diesel fuels [10]. Moreover, the *n*-heptane/toluene mixture is actively used as surrogate blend since it reproduces the properties of practical fuels better than iso-octane/*n*-heptane mixture [11]. Therefore, the combustion of toluene/*n*-heptane blends has been extensively investigated experimentally and numerically, see e.g. [12-16] and references therein. In particular, a number of works focus on auto-ignition of such blends using a HCCI engine [12], shock tubes [13] and rapid compression machines [14-15]. A detailed chemical kinetic model for *n*-heptane/isooctane/toluene mixtures has been proposed and validated comparing modeling results with available shock tube and flow tube data [16].

In spite of these efforts, current kinetic models do not allow an accurate prediction of the PAH concentration profiles and soot particle concentrations for various operation conditions. Widely accepted gas phase kinetic models of PAH formation [13, 17-18] do not contain components such as toluene and methylnaphthalene [19], which are important for practical fuels, or are either too large to be incorporated in reference fuel models [17-18], or were not validated on the experimental data for aromatic molecule concentrations [13]. Recently, a detailed reaction mechanism [19-20] was proposed for C_1 and C_2 hydrocarbon combustion and PAH growth up to five-ring aromatics, which does not have the disadvantages mentioned above. This mechanism was validated against the experimental data obtained in 19 different laminar flames for C_1, C_2 fuels and demonstrated a good qualitative and quantitative agreement with them.

Despite the fact that the soot formation is a critical problem, for example in aviation combustion chambers, measured concentration profiles of PAHs, which could be used for the surrogate model validations, can be only scarcely found in the literature. Xu et al. [21] measured the mole fraction profiles of intermediates in a fuel-rich *n*-heptane/toluene flame under low pressure conditions, which were, however, far from practical conditions. Therefore, the experimental investigation of *n*-heptane/toluene flame structure at higher pressures is of great importance.

In this study, we report the newly measured mole fraction profiles including PAH precursors in an atmospheric premixed burner-stabilized fuel-rich (φ = 1.75) *n*-heptane/toluene/O_2/Ar flame (*n*-heptane/toluene ratio is 7:3 by liquid volume). An extended reaction mechanism constructed on the basis of a detailed mechanism [19, 20, 22] is used to simulate the experimental data. The histories of reactions of aromatic molecule formation are examined and discussed.

Chemical Kinetic Mechanism Formulation

The reaction model used for the *n*-heptane/toluene mixture oxidation is a part of the global reaction data base at the DLR Institute of Combustion Technology. This kinetic data base has a hierarchical structure and is developed through continuous adaptation, extension, validation and optimization. The reaction database includes an inherently consistent body reaction model with submodels for H_2, CO, CH_4, CH_3OH, C_2H_4, C_2H_5OH, C_2H_6, C_3H_8, *n*-C_4H_{10}, C_7H_8, cy-C_6H_{12}, cy-C_9H_{18}, *n*-C_7H_{16}, *i*-C_8H_{18}, *n*-$C_{10}H_{22}$, *i*-$C_{10}H_{22}$, *i*-$C_{11}H_{24}$, *n*-$C_{12}H_{26}$ and *n*-$C_{16}H_{34}$. The core detailed reaction model consists of C_1-C_2 mechanism with PAH formation [19-20]. The feature of the *n*-C_7H_{16} sub-model is described elsewhere [22], the toluene sub-model is a part of the mechanism for PAH formation [19-20]. No changes were made to this mechanism. However, the *n*-heptane/toluene cross reactions have been added to the model to account for their influence on the fuel consumption rate. As the toluene is barely reactive at low temperature, we suppose that cross reactions can be important only between radicals and olefins produced by *n*-heptane decomposition and toluene (R1-R3) and their derivatives, i.e. benzyl (R5-R9) and phenyl (R4, R10-R15), see Table 1. The activation energies in the Arrhenius equation for the rate constants given in Table 1 were evaluated using the Polanyi-Semenov equation [23]. The pre-exponential A-factors follow paraffin oxidation data [23] and corrections for the entropy change.

In this section, the model validation against literature data on flame speed for toluene/air [24] and *n*-heptane/air [25-28] mixtures, shock tube auto-ignition for *n*-heptane/toluene mixture [29], PAH concentration profiles [30] and soot volume fractions [31] measured in *n*-heptane and toluene laminar premixed flames is shortly summarized. The laminar flame and ignition delay times simulations are performed with the PREMIX and SENKIN codes [32-33] of the CHEMKIN-II package.

Table 1
Cross reactions for *n*-heptane/toluene mixtures,
$k = A \cdot T^n \exp(-E_a/T)$ in cm^3, s, K

#	Reaction	A	*n*	E_a
1	$C_7H_8+C_7H_{15}=C_7H_7+C_7H_{16}$	7.00×10^{11}	0	5700
2	$C_7H_8+nC_3H_7=C_7H_7+C_3H_8$	3.00×10^{11}	0	5700
3	$C_7H_8+nC_4H_9=C_7H_7+nC_4H_{10}$	4.00×10^{11}	0	5700
4	$C_7H_{16}+A1\text{-}=C_7H_{15}+A1$	5.00×10^{11}	0	5500
5	$aC_7H_{14}+C_7H_7=C_7H_{13}+C_7H_8$	3.50×10^{11}	0	5500
6	$cC_7H_{14}+C_7H_7=C_7H_{13}+C_7H_8$	3.50×10^{11}	0	5500
7	$aC_6H_{12}+C_7H_7=C_6H_{11}+C_7H_8$	3.00×10^{11}	0	5600
8	$C_5H_{10}+C_7H_7=C_5H_9+C_7H_8$	2.00×10^{11}	0	5600
9	$C_4H_8+C_7H_7=nC_4H_7+C_7H_8$	1.50×10^{11}	0	5600
10	$aC_7H_{14}+A1\text{-}=C_7H_{13}+A1$	3.50×10^{11}	0	4850
11	$cC_7H_{14}+A1\text{-}=C_7H_{13}+A1$	3.50×10^{11}	0	4850
12	$aC_6H_{12}+A1\text{-}=C_6H_{11}+A1$	3.00×10^{11}	0	4850
13	$C_5H_{10}+A1\text{-}=C_5H_9+A1$	2.00×10^{11}	0	4400
14	$C_4H_8+A1\text{-}=nC_4H_7+A1$	1.50×10^{11}	0	4900
15	$A1\text{-}+C_3H_6=A1C_2H_3+CH_3$	1.50×10^{11}	0	5350

Figure 1 illustrates a good agreement between experimental data for laminar flame speeds of toluene/air [24] and *n*-heptane/air [25-28] mixtures and model predictions. The model also provides a good fit of the measured ignition delay times for *n*-heptane/toluene mixtures [29] (Fig. 2). Figure 3 shows a comparison of mole fraction profiles of aromatic molecules measured in a laminar premixed *n*-heptane flame [30] with the model predictions. The modeling was performed with the thermocouple data corrections, but the large uncertainty in the temperature data [30] should be noted. The predictions and measurements [31] of soot volume fractions in the laminar toluene flames are shown in the Fig. 4. For these simulations the soot model of Frenklach and co-authors was used [34]. Therefore, the comparison of the simulations with the literature experimental data demonstrates the high performances of the chemical kinetic mechanism in reproducing the combustion characteristics of the fuels studied. The influence of the cross reactions introduced on the combustion features is negligible.

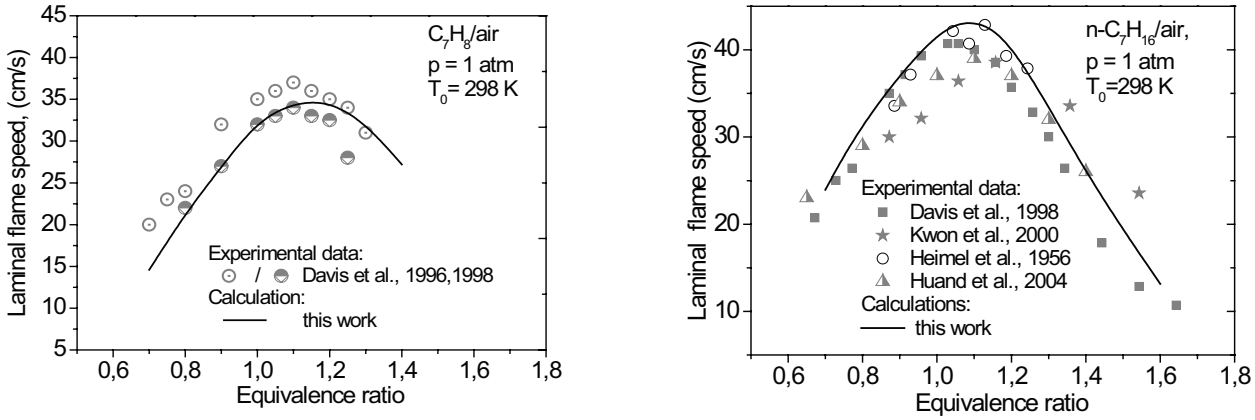

Fig. 1. Comparisons of experimental data and simulation results for laminar flame speed of toluene [24] (top) and *n*-heptane [25-28] (bottom).

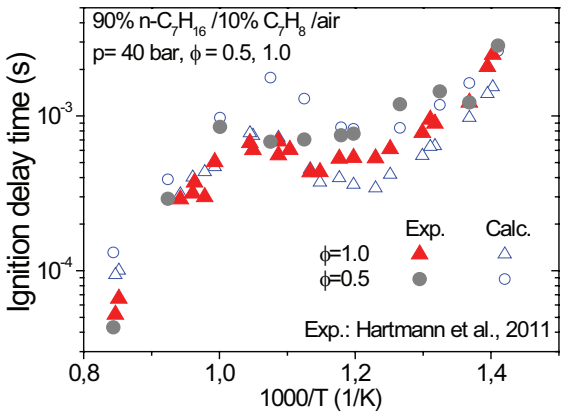

Fig. 2. Measured [29] ignition delay time for *n*-heptane/toluene mixture compared to calculations.

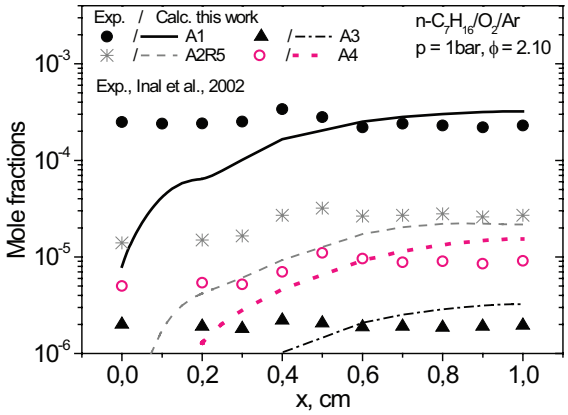

Fig. 3. Comparison of mole fraction profiles of aromatic molecules measured in a laminar premixed *n*-heptane/O_2/Ar flame [30] with the model predictions.

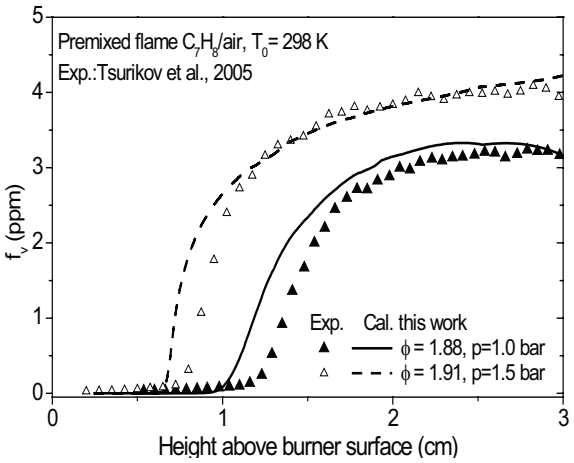

Fig. 4. Soot volume fractions measured in the laminar premixed toluene/air flame [31] compared against simulations performed using the reaction model coupled with the soot model.

Experimental

A fuel-rich premixed flame of *n*-heptane/toluene/O_2/Ar is stabilized on a Botha-Spalding flat burner at atmospheric pressure. The burner consists of a perforated (0.5 mm orifices with 0.7 mm center-to-center spacing) brass disc 16 mm in diameter and 3 mm thick embedded in a brass housing surrounded by a jacket for the circulation of a thermostating liquid (polymethylsiloxane temperature kept at 120 °C). The flows of argon and oxygen are adjusted by the calibrated mass-flow controllers (MKS Instruments Inc.). *n*-Heptane and toluene are premixed (liquids volume ratio was 7:3, respectively) and supplied into a vaporizer through a steel capillary using a syringe pump driven by a stepper motor. The vaporizer consists of a pyrex vessel filled with steel beads and heated by electrical coil. The temperature of the vaporizer is kept at 90 °C. This temperature is high enough to evaporate completely *n*-heptane and toluene coming into the vaporizer in unit time, while at the same time does not exceed the boiling temperatures (98.42 °C for *n*-heptane and 110.6 °C for toluene) to prevent boiling of liquids in the capillary (that could cause instabilities in the fuel vapor supply to the burner). Argon is supplied into the vaporizer. The line between the vaporizer and the burner has an inlet for the oxygen supply to the gaseous *n*-heptane/toluene/Ar mixture. This line is maintained at 120 °C by an electrical heater. The temperatures of the burner housing, the line, and the vaporizer is controlled by T-type thermocouples.

The flame has the following mole composition: *n*-heptane/toluene/O_2/Ar = 2.29/1.36/21.36/75 % (equivalence ratio φ = 1.75). The total flow rate of the unburnt mixture is 0.92 slpm.

Flame sampling molecular beam mass spectrometry (MBMS) with soft ionization by electron impact is used for measurements of species mole fractions in the flame as a function of the height above burner (HAB). Detailed description of the MBMS setup is given elsewhere [35]. It has been used previously to measure atmospheric-pressure flame structures, see, e.g., [36]. Flame sample is extracted from the burning area by a quartz cone nozzle with 40° inner angle and 0.08 mm orifice diameter. The wall thickness at the nozzle tip is 0.08 mm to minimize heat loss from the sampling area into the nozzle and to produce minimal flame perturbations. The gas sample forms a molecular beam that passes through a skimmer, molecular beam modulator and collimator before entering a region of soft ionization by electrons (spread in ionization energies of ±0.25 eV, the basis width of the electron energy distribution function). Ions are collected and analyzed by a quadrupole mass-spectrometer. Electron energies are selected for each species analyzed in order to obtain a signal-to-noise ratio high enough, without interferences from fragmentation of other species.

Deriving mole fraction profiles for intermediate species from the mass peak intensity profiles has been achieved using the procedure proposed by Cool et al. [37]. A similar procedure was used and described in details in our previous work [36], and it is described only briefly below.

The sensitivity factor (S) links the signal intensity (I) with the mole fraction (X) for each species at a given temperature and pressure by a simple relation: I = SX. *S* is proportional to $\sigma(E)$, the ionization cross-section at electron energy *E*. Thus, we can evaluate the mole fraction of each intermediate species X_i using the following relation: $I_i/I_S = [\sigma_i(E_i)/\sigma_S(E_S)][X_i/X_S]$, where index *i* corresponds to intermediate species, and the index *S* corresponds to the nearest stable species with known mole fraction. The electron ionization cross sections at a given electron energy are calculated using NIST Electron Impact Cross Section Database [38]. For species for which data were not available in the NIST database, ionization cross sections were estimated by the method described in [39]. Mole fractions of reactants are determined using calibration gas mixtures of known composition. Mole fraction of major products (CO, CO_2, H_2, H_2O) are evaluated using the abovementioned relation and material balance equations for C, O and H elements.

The uncertainty of the determination of mole fraction of the flame reactants and major products (CO, CO_2, H_2O, H_2) is estimated to be ±15% of the maximum mole fraction values. For other species, mole fractions are determined to within a factor of about 2.

Temperature profiles in the flames are measured by a Pt/Pt + 10% Rh thermocouple with SO_2 anticatalytic coating. The procedure of its manufacturing as well as its dimensions are described in [36]. The flame temperature profile is measured with the thermocouple junction located at 0.2 mm from the sampling nozzle tip. The radiation heat losses by the thermocouple are taken into account as described elsewhere [40-41]. The measured temperature profiles were used as input data for the flame structure simulations. Gas-dynamic perturbations of the flame by the sampling probe were taken into account similarly as it was done in our previous works [36, 42] by shifting all the mole fraction profiles measured upstream by the distance $Z \sim d\bullet(Q/(S\bullet V))^{0.5}$, where d is the diameter of the orifice, Q is the volumetric flow rate though the orifice, S is the area of the orifice and V is the linear velocity of the flow riding onto the probe [43]. The maximum shift corresponds to the position of the probe near the burner and does not exceed 0.3 mm.

Results and Discussion

Simulated and experimental mole fraction variations vs. height above burner (HAB) for reactants and major products in the flame are given in Fig. 5. This figure also shows the measured temperature profile of the flame. As can be seen from the Fig. 5, the mechanism reproduces satisfactorily the concentration profiles of *n*-heptane, toluene, CO_2, CO, O_2, H_2O. Some discrepancies are observed between the measurements and the simulation results for H_2. This can be explained by high background signal at the mass peak m/z = 2 due to the high diffusivity of hydrogen and, therefore, insufficient rate of H_2 evacuation from the vacuum system.

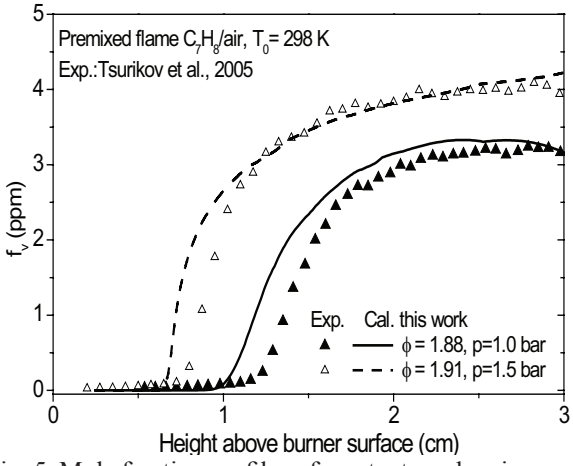

Fig. 5. Mole fraction profiles of reactants and major products in *n*-heptane/toluene/O_2/Ar flame. Symbols: experiment; curves: modeling.

Figure 6 shows comparisons of the experimentally detected and simulated profiles of the species mole factions for: methane CH_4, ethylene C_2H_4, acetylene C_2H_2, propargyl C_3H_3, diacetylene C_4H_2, vinylacetylene C_4H_4, 1,3-butadiene C_4H_6, cyclopentadienyl C_5H_5, benzene C_6H_6, phenol C_6H_5OH, styrene $C_6H_5C_2H_3$. The species related to mass peaks 40 (allene+propyne), 42 (propene+ketene), 56 (1-butene+2-butene), and 70 (1-pentene+2-pentene) are not separated due to the very close difference between the ionization potentials of corresponding components. Measured and predicted profiles of combined mole fraction of these species are also given in Fig. 6.

As can be seen from the figure, the mechanism used predicts well the mole fraction profiles for the following intermediates measured: ethylene, butene (combination of isomers), phenol, styrene. However, it should be noted that for a few species (acetylene, diacetylene, 1-pentene+2-pentene) the mechanism does not provide an even qualitative agreement with the experimental data. In particular, the measurements demonstrate that acetylene and diacetylene are consumed completely in the post flame zone, however the model predicts a relatively high level of their mole fraction in this zone. Moreover, the model significantly overpredicts the maximum mole fraction of these species. For other intermediates, the model provides a good qualitative prediction of their mole fraction profiles, however it is not adequate in predicting their maximum mole fractions in the flame. It overpredicts more than twice the peak mole fractions for methane, propargyl, 1,3-butadiene, benzene; it underpredicts more than 2 times the peak mole fractions for propene+ketene, vinylacetylene, cyclopentadienyl.

Detailed sensitivity analyses and comparisons of experimental and simulation results revealed that the shortcomings of the mechanism mentioned above can be overcome rather easily. First, the reaction paths to pentene which have been excessively removed previously during the mechanism development [22] should be re-introduced in the model and second, the rate coefficients of the following reactions:

$C_4H_2+OH<=>C_3H_2+HCO;$
$H_2CCCH+OH<=>HCO+C_2H_3;$
$H_2CCCH+O<=>CH_2O+C_2H;$
$H_2CCCH+H(+M)<=>C_3H_4(+M);$
$C_4H_2+H<=>H_2CCCCH;$
$H_2CCCCH+O_2<=>CH_2CO+HCCO;$
$C_2H_2+OH<=>C_2H+H_2O;$
$C_2H_2+C_2H<=>C_4H_2+H,$

which follow mostly from [44], should be revised in light of the new data set, too.

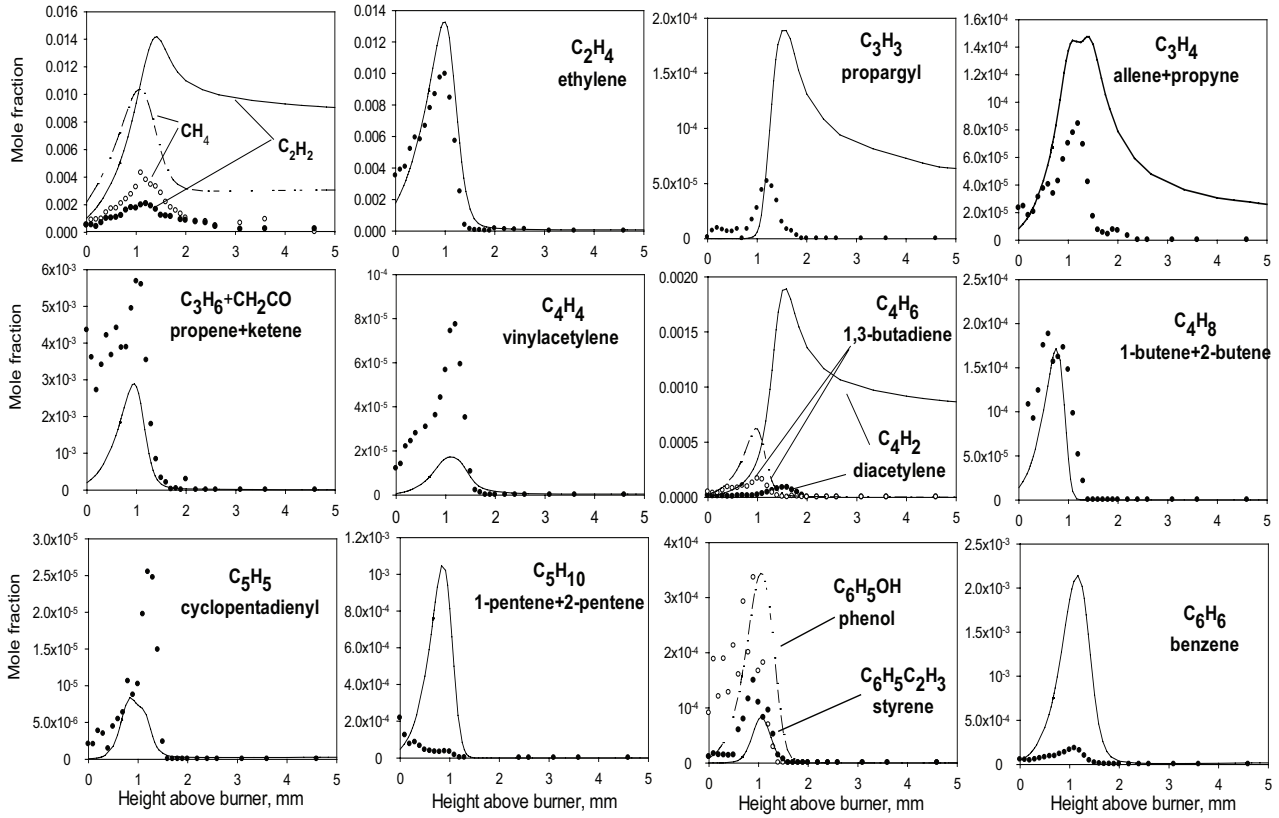

Fig. 6. Mole fraction profiles of the main intermediates in premixed *n*-heptane/toluene/O_2/Ar flame. Symbols: experiment; curves: modeling.

To identify the reactions which have the most significant effects on the rate of benzene formation in the *n*-heptane/toluene flame studied in this work, a reaction path analysis is carried out. First, to better understand the origin of aromatic molecules formation, the pathways leading to benzene and phenyl formation in the *n*-heptane flame [30] (Fig. 3) and in the toluene flame [31] (Fig. 4) are analyzed (Fig. 7) and then compared with those in the *n*-heptane/toluene flame studied (Fig. 8). That can be done, because the parameters of these flames are sufficiently similar. Three different flame zones (and flame temperatures) are examined: Preheat zone, main reaction zone, and post-flame zone. The thickness and color of pointers in Fig. 7 and 8 provide insights about the importance of the different reaction pathways and their relation to the flame zones. The darkest color corresponds to the post flame zone.

Figure 7 illustrates that in the toluene flame the first aromatic ring formation in the preheat and main reaction zone occurs mostly through the reactions of H atom abstraction from toluene and reactions of benzyl radical with HO_2. In the post flame zone the reaction C_7H_8+H <=> A1+CH_3 dominates this process; propargyl radical recombination reaction becomes important as well.

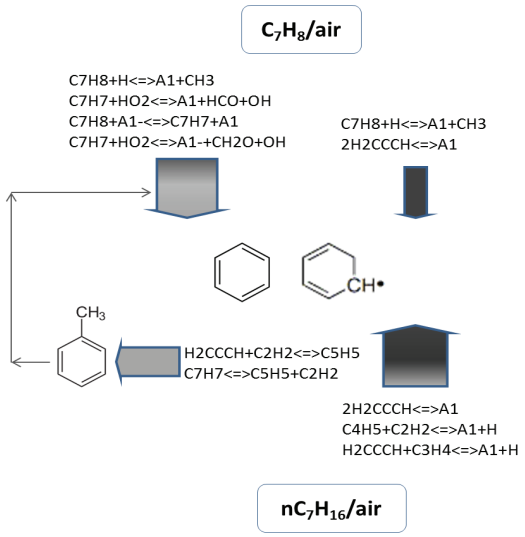

Fig. 7. Schematic showing the reaction paths of formation of the first aromatic rings in toluene flame [31] versus *n*-heptane flame [30].

Unlike in the toluene flame, in the *n*-heptane flame, reactions of the small resonantly-stabilized radicals are the main routes to benzene (Fig. 7). The second non-negligible channel to the first aromatic

ring formation is the benzyl production by recombination of cyclopentadienyl radicals with acetylene (Fig. 7). This route is most observable in the first flame zone.

As shown in Fig. 8 in the *n*-heptane/toluene flame the reaction paths to benzene are mostly similar to those plotted for the toluene flame in the Fig. 7. However in this case, in the post-flame zone, the reaction $2H_2CCCH$ <=> A1 dominates and reaction C_7H_7+HO_2 <=> A1+HCO+OH becomes important as well. That can be explained with the high concentration of C_7H_7, which is produced in two parallel channels during the early stages of combustion: In the reactions of H abstraction from toluene and in the reaction C_7H_7 <=> C_5H_5+C_2H_2, Fig. 7. This means that the benzene formation pathways in the flame studied represent the combinations of routes observed in the individual flames, but dominated by the typical of reaction paths of the toluene flame.

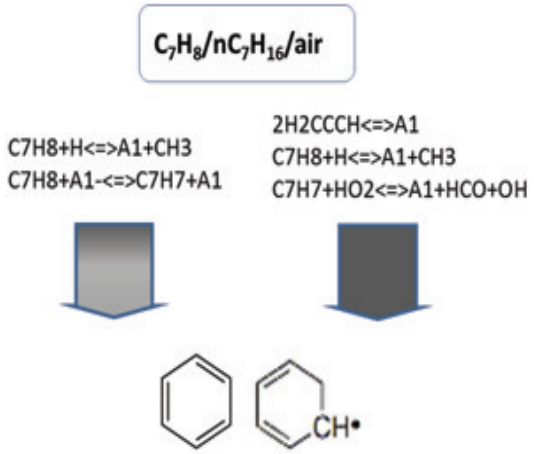

Fig. 8. Main reaction paths of the first aromatic rings formation in the *n*-heptane/toluene flame studied in this work.

Conclusion

Mole fraction profiles of reactants and intermediate species including PAH precursors were newly measured in a premixed fuel-rich (φ = 1.75) *n*-heptane/toluene/O_2/Ar flame at atmospheric pressure. A detailed chemical kinetic mechanism, developed earlier, for *n*-heptane/toluene combustion and the PAH formation was extended with cross reactions for *n*-heptane and toluene derivatives and used for simulations of new experimental data. The analysis of the reaction pathways has shown that in the flame of the *n*-heptane/toluene blend (7:3 liquid ratio) the reactions dominant for the formation of the first aromatic ring (benzene and phenyl) were as those typical for pure toluene flames. Although the agreement between measurements and simulations is sufficiently good, the discrepancies observed between the measured and calculated mole fractions demonstrated a need of additional improvements of the mechanism, however, this is a topic of our future research. To our knowledge, the measurements of mole fraction profiles of PAH and intermediates reported here, are the first of its kind and represent an unique data set extremely important for validation of chemical kinetic mechanisms for practical fuels.

Acknowledgements

This work was partially supported by Russian Foundation of Basic Research under Grant No. 12-03-31246-a and EU Project FP7-265848-FIRST (Fuel Injector Research for Sustainable Transport).

References

[1]. W.J. Pitz, C.J. Mueller, Prog. Energy Comb. Sci. 37 (3) (2011) 330–350.
[2]. N.A. Slavinskaya, U.Riedel, E.Saibov, K. Kannaiyan, AIAA-2012-0977, 50th Aerospace Science Meeting & Exhibit, Nashville, TN, USA, 2012.
[3]. H.F. Calcote, D.M. Manos, Combust. Flame 49 (1-3) (1983) 289–304.
[4]. M. Frenklach, H. Wang, in: H. Bockhorn (Ed.), Detailed Mechanism and Modeling of soot particle formation, Springer-Verlag Berlin, Springer Series in Chemical Physics, 1994, Vol. 59, p. 165.
[5]. H. Richter, J.B. Howard, Prog. Energy Comb. Sci. 26 (4-6) (2000) 565-608.
[6]. M. Frenklach, Phys. Chem. Chem. Phys. 4 (11) (2002) 2028–2037.
[7]. P. Dagaut, M. Cathonnet, Prog. Energy Comb. Sci. 32 (1) (2006) 48–92.
[8]. S. Dooley, S.H. Wona, J. Heyne, T.I. Farouk, Y. Ju, F.L. Dryer, K. Kumar, X. Hui, C.-J. Sung, H. Wang, M.A. Oehlschlaeger, V. Iyer, S. Iyer, T.A. Litzinger, R.J. Santoro, T. Malewicki, K. Brezinsky, Combust. Flame 159 (4) (2012) 1444–1466.
[9]. C.V. Naik, A.M. Dean, Combust. Flame 145 (1-2) (2006) 16–37.
[10]. J.T. Farrell, N.P. Cernansky, F.L. Dryer, D.G. Friend, C.A. Hergart, C.K. Law, R.M. McDavid, C.J. Mueller, A.K. Patel, H. Pitsch, SAE Paper, 2007-01-0201, 2007.

[11]. G.T. Kalghatgi, SAE Paper 2005-01-0239, 2005.
[12]. J.C.G. Andrae, D. Johansson, P. Björnbom, P. Risberg, G. Kalghatgi, Combust. Flame 140 (4) (2005) 267-286.
[13]. G.L. Agafonov, I. Naydenova, P.A. Vlasov, J. Warnatz, Proc. Combust. Inst. 31 (2007) 575–583.
[14]. R. Di Sante, Combust. Flame 159 (1) (2012) 55–63.
[15]. G. Vanhove, G. Petit, R. Minetti, Combust. Flame 145 (3) (2006) 52–532.
[16]. Y. Sakai, A. Miyoshi, M. Koshi, W.J. Pitz, Proc. Combus. Inst. 32 (2009) 411–418.
[17]. N.M. Marinov, W.J. Pitz, C.K. Westbrook, M.J. Castaldi, S.M. Senkan, Comb. Sci. and Tech. 116-117 (1-6) (1996) 211–287.
[18]. J. Appel, H. Bockhorn, M. Frenklach, Combust. Flame 121 (1-2) (2000) 122–136.
[19]. N.A. Slavinskaya, U. Riedel, S.B. Dworkin, Q. Zhang, M.J. Thomson, Combust. Flame 159 (3) (2012) 979–995.
[20]. N.A. Slavinskaya, P. Frank, Combust. Flame 156 (9) (2009) 1705–1722.
[21]. H. Xu, C. Yao, G. Xu, Z. Wang, H. Jin, Combust. Flame 160 (8) (2013) 1333–1344.
[22]. N.A. Slavinskaya, B. Noll, Proceedings of GT2006ASME Turbo Expo 2006, GT2006-90958, Barcelona, Spain, 2006.
[23]. E.T. Denisov, O.M. Sarkisov, G.I. Likhtenshtein, Chemical Kinetics: Fundamentals and Recent Developments, Elsevier Science, New York, NY, USA, 2003.
[24]. S.G. Davis, C.K. Law, Combust. Sci. and Tech. 140 (1-6) (1998) 427–449.
[25]. S. Heimel, R.C. Weast, Proc. Combust. Inst. 6 (1) (1956) 296–302.
[26]. S.G. Davis, C.K. Law, Proc. Combust. Inst. 27 (1) (1998) 521–527.
[27]. O.C. Kwon, M.I. Hassan, G.M. Faeth, J. Prop. Power 16 (3) (2000) 513–522.
[28]. Y. Huang, C.J. Sung, J.A. Eng, Combust. Flame, 139 (3) (2004) 239–251.
[29]. M. Hartmann, I. Gushterova, M. Fikri, C. Schulz, R. Schießl, U. Maas, Combust. Flame 158 (1) (2011) 172–178.
[30]. F. Inal, S.M. Senkan, Combust. Flame 131 (1-2) (2002) 16–28.
[31]. M. Tsurikov, K.P. Geigle, V. Krüger et al, Combust. Sci. and Tech. 177 (10) (2005) 1835–1862.
[32]. R.J. Kee, F.M. Rupley, J.A. Miller, One-dimensional premixed laminar flame code, CHEMKIN-II Version 2.5b, 1992.
[33]. A.E. Lutz, R.J. Kee, J.A. Miller, SENKIN: a FORTRAN program for predicting homogeneous gas phase chemical kinetics with sensitivity analysis, Report No. SAND87-8248, Sandia National Laborotories, 1994.
[34]. M. Frenklach, H. Wang, in: H. Bockhorn (Ed.), Detailed Mechanism and Modeling of soot particle formation, Springer-Verlag, Berlin, Springer Series in Chemical Physics, 1994, p. 165.
[35]. O.P. Korobeinichev, S.B. Ilyin, V.V. Mokrushin, A.G. Shmakov, Combust. Sci. Technol. 116-117 (1-6) (1996) 51–67.
[36]. I.E. Gerasimov, D.A. Knyazkov, S.A. Yakimov, T.A. Bolshova, A.G. Shmakov, O.P. Korobeinichev, Combust. Flame 159 (5) (2012) 1840–1850.
[37]. T.A. Cool, K. Nakajima, K.A. Taatjes, A. McIlroy, P.R. Westmoreland, M.E. Law, A. Morel, Proc. Combust. Inst. 30 (2005) 1681–1688
[38]. Y.-K. Kim, K.K. Irikura, M.E. Rudd, M.A. Ali, P.M. Stone, J. Chang, J.S. Coursey, R.A. Dragoset, A.R. Kishore, K.J. Olsen, A.M. Sansonetti, G.G. Wiersma, D.S. Zucker, M.A. Zucker, http://physics.nist.gov/PhysRefData/Ionization.
[39]. W.L. Fitch, A.D. Sauter, Anal. Chem. 55 (6) (1983) 832–835.
[40]. W.E. Kaskan, Proc. Combust. Inst. 6 (1957) 134–141.
[41]. C.R. Shaddix, Correcting thermocouple measurements for radiation loss: a critical review, Proceedings of the 33rd National Heat Transfer Conference, HTD99-282, Albuquerque, New Mexico, 1999.
[42]. A.G. Shmakov, O.P. Korobeinichev, I.V. Rybitskaya, A.A. Chernov, D.A. Knyazkov, T.A. Bolshova, A.A. Konnov, Combust. Flame 157 (3) (2010) 556–565.
[43]. O.P. Korobeinichev, A.G. Tereshchenko, I.D. Emel'yanov, A.L. Rudnitskii, S.Y. Fedorov, L.V. Kuibida, V.V. Lotov, Combust. Explo. Shock Waves 21 (5) (1985) 524–530.
[44]. D.L. Baulch, C.T. Bowman, C.J. Cobos, R.A. Cox, Th. Just, J.A. Kerr, M.J. Pilling, D. Stocker, J. Troe, W. Tsang, R.W. Walker, J. Warnatz, J. Phys. Chem. Ref. Data 34 (3) (2005) 757.

Received 21 March 2014